Radiative Boundary Layer Flow and Heat Transfer of Nanofluid over a Nonlinear Stretching Sheet with Slip Conditions and Suction

T. Vijaya Laxmi [a, b, *], Bandari Shankar [a]

[a] *Department of Mathematics, Osmania University, Hyderabad-500007, Telangana, India.*

[b] *Department of Mathematics, M.V.S. Govt. Arts & Science College, Mahabubnagar-509001, Telangana, India*

Abstract

The magneto hydrodynamics (MHD) boundary layer flow and heat transfer of a nanofluid   with boundary slip condition for velocity second order, thermal slip, solutal slip, and suction, thermal radiation have been investigated numerically over a nonlinear stretching sheet with viscous dissipation. The profiles for the velocity, temperature and nanoparticle concentration depends on parameters viz. thermal radiation parameter R, suction parameter s, velocity first and second order slip parameters A and B, respectively, thermal slip parameter C, concentration slip parameter D, power-law parameter N, Prandtl number Pr, Lewis number Le, Brownian motion parameter Nb, thermophoresis parameter Nt, Eckert number Ec, and magnetic parameter M. Similarity transformation is used to convert the governing non-linear boundary-layer equations into coupled higher order non-linear ordinary differential equations. These equations are numerically solved by using an implicit finite difference method known as Keller-Box method. An analysis has been carried out to reveal the effects of governing parameters corresponding to various physical conditions. Numerical results and Graphical representation are obtained for distributions of velocity, temperature and concentration, as well as, for the skin friction, local Nusselt number and local Sherwood number for several values of governing parameters. The result reveals that velocity decreases with increase of first and second order velocity slip, suction and increases with increase of power-law parameter. Temperature decreases with the increase of thermal slip, suction, concentration slip but increases with thermal radiation, second order velocity slip. Nanoprticle concentration decreases with increase of concentration slip, suction, thermal radiation, thermal slip but increase with increase of second order velocity slip. A comparison with previous results available in the literature has been done and we found a good conformity with it. The numerical values of skin friction, Nusselt number and Sherwood number are presented in tables.

1. Introduction

Boundary layer flow over a stretching surface with velocity slip, temperature-jump and solutal slip boundary conditions is an important type of flow and heat transfer occurring in several engineering applications. In these types of transport phenomena, the equations corresponding to continuum equations of momentum and energy are still governed by the Navier-Stokes equations, but the effects of the walls are taken into account by using appropriate boundary conditions. No-slip condition is inadequate for most non-Newtonian liquids, as some polymer melt often shows microscopic wall slip and that has a controlling influence by a nonlinear and monotone relation between the slip velocity and the traction. It is known that, a viscous fluid normally sticks to boundary and there is no slip of the fluid relative to the boundary. However, in some situations there may be a partial slip between the fluid and the boundary. For such fluid, the motion is still governed by the Navier Stokes equations, but the usual no-slip condition at the boundary is replaced by the slip condition. Partial velocity slip may occur on the stretching boundary when the fluid is particulate, such as emulsions, suspensions, foams and polymer solutions. In various industrial processes, slip effects can arise at the boundary of the pipes, walls, curved surfaces etc. A boundary layer slip flow problem arises in polishing of artificial heart valves and internal cavities. Recently many authors obtained analytical and numerical solutions for boundary layer flow and heat transfer due to a stretching sheet with slip boundary conditions.

Some of the authors have considered second order slip boundary conditions to study the flow, heat and mass transfer by employing boundary layer approximations and seeking similarity solutions [1-5]. Khader [6] obtained

---

[*] Corresponding author. e-mail: vijaya9966998024@rediffmail.com, bandarishankar@gmail.co.in.

numerical solution by Laguerre collocation method to study the effect of viscous dissipation on the steady flow with heat transfer of Newtonian fluid towards a permeable stretching surface embedded in a porous medium with second order slip effect. Abdul Hakeem et al. [7] performed both numerical and analytical solution to study the effect of magnetic field on a steady two dimensional laminar radiative flow of an incompressible viscous water based nanofluid over a stretching/shrinking sheet with second order slip boundary condition. Very recently, Mabood and Mastroberardinob [8] considered the second order slip boundary conditions to investigate the effects of viscous dissipation and melting on MHD boundary layer flow of an incompressible, electrically conducting water-based nanofluid over a stretching sheet. Hayat et al. [9] studied a steady three-dimensional boundary layer flow of water based nanofluid with copper as nanoparticle over a permeable stretching surface with second order velocity slip and homogeneous–heterogeneous reactions. Zhu et al. [10] investigated the effects of the second-order velocity slip and temperature jump boundary conditions on the magnetohydrodynamic (MHD) flow and heat transfer of water-based nanofluids containing Cu and Al_2O_3 in the presence of thermal radiation. Megahed [11] obtained numerical solution to study the boundary layer flow and heat transfer for an electrically conducting Casson fluid over a permeable stretching surface with second-order slip velocity model and thermal slip conditions in the presence of internal heat generation/absorption and thermal radiation.

Heat transfer, influenced by thermal radiation has applications in many technological processes, including nuclear power plants, gas turbines and various propulsion devices for aircraft, missiles, satellites and space vehicles. Various engineering processes, involve high temperature and essential to the study of radiation heat transfer in designing and manufacturing of equipments. Suspension of nano-solid particles in classical fluids has a known method for the improvement of thermal conductivity of heat transfer fluids. 'Nanofluid', introduced by Choi et al. [12], gives the fluid contains of nano-sized particles (diameter of 1 to 100 nm) that are suspended in a base fluid, like water, ethylene glycol, propylene glycol, etc. Addition of high thermally conductive metallic nanoparticles, like silver, copper, aluminium, silicon, improves thermal conductivity of such mixtures, thereby enhancing the overall energy transport capability. It has been found that nanofluids have a potential to increase the thermal conductivity as well as convective heat transfer performance of the base fluid. One of the possible mechanisms for anomalous increase in the thermal conductivity of nanofluids is the Brownian motion of the nanoparticles within the base fluids. This attractive characteristic of nanofluids creates an impressive for wide application [13], [14]. Nanofluids became the next-generation heat transfer fluids and their superior heat transfer features are better than that of any other ordinary fluids. Khan and Pop [15] studied the phenomenon of nanofluid over a stretching sheet for laminar boundary layer flow. The nanofluid flow over an exponentially stretching sheet was introduced by Nadeem and Lee [16]. The laminar boundary layer flow of a nanofluid over a nonlinear stretching sheet is extended by Rana and

Bhargava [17]. Rahman and Eltayeb [18] extend the radiative heat transfer in a hydromagnetic nanofluid over a nonlinear stretching surface. Cortell et al. [19] explained the boundary layer flow and heat transfer of fluid under the consideration of thermal radiation and viscous dissipation over a nonlinear stretched sheet. The boundary layer flow over a permeable moving flat plate under the effect of viscous dissipation and thermal radiation by considering of few nanofluids is studied by Motsumi and Makinde [20]. Heat transfer over nonlinear stretching and shrinking sheets under the influence of magnetic field, thermal radiation and viscous dissipation by considering copper, alumina, and titanium oxide nanoparticles was examined by Pal et al. [21]. Later, Nandy and Pop [22] extended the study of MHD boundary layer stagnation flow and heat transfer over a shrinking sheet incorporating the two component model under the effect of radiation. Rashidi et al. [23] have also investigated the combined effect of magnetic field and thermal radiation over a vertical stretching sheet for two dimensional water based nanofluid flow. Mustafa et al. Studied [24] the boundary layer flow of a nanofluid over an exponentially stretching sheet to the case of a permeable shrinking sheet with the second order velocity slip in the presence of zero normal flux of the nanoparticles at the boundary. Several authors have studied the flow and heat transfer of a viscous (regular) fluid over an exponentially stretching surface ([25]; [26]; [27]; and [28]).

Based on the observations from the above cited work, the purpose of the present paper is to analyze the effect of second order velocity slip, temperature slip and solutal slip in the presence of thermal radiation with suction of a steady two-dimensional flow of a nanofluid over a nonlinear stretching sheet. Governing nonlinear ordinary differential equations obtained after the application of similarity transformations are solved numerically by means of Keller-Box method. The effects of different flow parameters on flow fields are elucidated through graphs and tables.

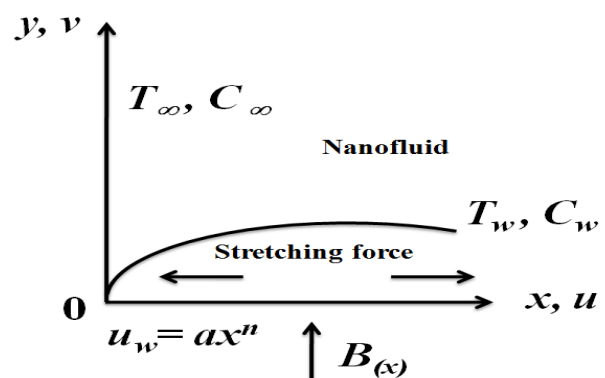## 2. Flow Analysis and Mathetatical Formulation

Figure 1. Flow organization with coordinate system

Consider a two dimensional, steady and incompressible viscous flow of a nanofluid past over a nonlinear stretching surface. The sheet is extended with velocity

$u_w(x) = ax^n$ with fixed origin location, where "n" is a nonlinear stretching parameter, "a" is a dimensional constant known as stretching rate and x is the coordinate measured along the stretching surface. The nanofluid flows at y = 0, where y is the coordinate normal to the surface. The fluid is electrically conducted due to an applied magnetic field B(x) normal to the stretching sheet. The magnetic Reynolds number is assumed small and so, the induced magnetic field can be considered to be negligible. The wall temperature T_w and the nanoparticle fraction C_w are assumed constant at the stretching surface. When y tends to infinity, the ambient values of temperature and nanoparticle fraction are denoted by $T\infty$ and $C\infty$, respectively. The constant temperature and nanoparticle fraction of the stretching surface T_w and C_w are assumed to be greater than the ambient temperature and nanoparticle fraction T_∞, C_∞, respectively. T is the temperature and C is the rescaled nanoparticle volume fraction in the boundary layer. The coordinate system and the flow model are shown in Figure 1. The governing equations of continuity, momentum, thermal energy and nanoparticles equations can be written as:

$$\frac{\partial u}{\partial x} + \frac{\partial v}{\partial y} = 0 \tag{1}$$

$$u \frac{\partial u}{\partial x} + v \frac{\partial u}{\partial y} = \upsilon \frac{\partial^2 u}{\partial y^2} - \frac{\sigma B^2(x)}{\rho_f} u \tag{2}$$

$$u \frac{\partial T}{\partial x} + v \frac{\partial T}{\partial y} = \alpha \frac{\partial^2 T}{\partial y^2} + \tau \left\{ D_B \frac{\partial C}{\partial y} \frac{\partial T}{\partial y} + \frac{D_T}{T_\infty} \left(\frac{\partial T}{\partial y} \right)^2 \right\}$$
$$+ \frac{\upsilon}{c_p} \left(\frac{\partial u}{\partial y} \right)^2 - \frac{1}{(\rho c)_p} \left(\frac{\partial q_r}{\partial y} \right) \tag{3}$$

$$u \frac{\partial C}{\partial x} + v \frac{\partial C}{\partial y} = D_B \frac{\partial^2 C}{\partial y^2} + \left(\frac{D_T}{T_\infty} \right) \frac{\partial^2 T}{\partial y^2} \tag{4}$$

The boundary conditions for the velocity, temperature and nanoparticle fraction are defined as:

$$u(x) = u_w + u_{slip}, \quad v = v_w(x),$$
$$T = T_w + T_{slip}, \quad C = C_w + C_{slip} \tag{5}$$
$$at \quad y = 0$$

$$u = 0, \quad v = 0, \quad T = T_\infty, \quad C = C_\infty \quad at \quad y = \infty \tag{6}$$

Here, u and v are the velocity components along the x and y-axes, respectively.

$\alpha = \dfrac{k}{(\rho c)_f}$ is the thermal diffusivity, σ is electrical conductivity, ν is the kinematic viscosity, ρ_f is the density of the base fluid, D_B is the Brownian diffusion coefficient and D_T is the thermophoresis diffusion coefficient.

$\tau = \dfrac{(\rho c)_p}{(\rho c)_f}$ is the ratio between the effective heat capacity of the nanoparticle material and heat capacity of the fluid, c is the volumetric volume coefficient, ρ_p is the density of the particles, and C is rescaled nanoparticle volume fraction. We assume that the variable magnetic

field B(x) is of the form $B(x) = B_0 x^{\frac{(n-1)}{2}}$. U_{slip} is the slip velocity at the surface and it is negative due to stretching. Wu's [29] slip velocity model used in this paper and is valid for arbitrary Knudsen numbers and is given as follows:

$$T_{slip} = k_1 \frac{\partial T}{\partial y} \qquad C_{slip} = k_2 \frac{\partial C}{\partial y}$$

where k_n is the Knudsen number, $l = \min(1/K_n, 1)$, σ is the momentum accommodation coefficient with $0 \leq \sigma \leq 1$ and γ is the molecular mean free path. Based on the definition of l, it is seen that for any given value of K_n, we have $0 \leq l \leq l$. Since the molecular mean free path γ is always positive it results that B is a negative number. A′, B′ are first and second order velocity slip factors, respectively, k1 is the thermal slip factor, k2 is the concentration slip factor.

Using the Rosseland [30] approximation as in Cortell [19], the radiative heat flux is simplified as:

$$q_r = -\frac{4\sigma^*}{3k^*} \frac{\partial T^4}{\partial y} \quad \cdots\cdots\cdots\cdots \text{(7)}$$

We assume that the temperature differences within the flow region, namely, the term T^4 can be expressed as a linear function of temperature. The best linear approximation of T^4 is obtained by expanding it in a Taylor series about $T\infty$ and neglecting higher order terms. That is:

$$T^4 \cong 4T_\infty^3 T - 3T_\infty^4 \quad \cdots\cdots\cdots\cdots \text{(8)}$$

Using equation (8) into equation (7) the modified equation of (3) is:

$$q_r = \frac{-4\sigma^*}{3k^*} \frac{\partial}{\partial v} \left(4T_\infty^3 - 3T_\infty^4 \right) = \frac{-16\sigma^* T_\infty^3}{3k^*} \frac{\partial T}{\partial y}$$
$$and \quad \frac{\partial q_r}{\partial y} = \frac{-16\sigma^* T_\infty^3}{3k^*} \frac{\partial^2 T}{\partial y^2} \tag{9}$$

$$u \frac{\partial T}{\partial x} + v \frac{\partial T}{\partial y} = \alpha \left(1 + \frac{4}{3} R \right) \frac{\partial^2 T}{\partial y^2} +$$
$$\tag{10}$$
$$\tau \left\{ D_B \frac{\partial C}{\partial y} \frac{\partial T}{\partial y} + \frac{D_T}{T_\infty} \left(\frac{\partial T}{\partial y} \right)^2 \right\} + \frac{\upsilon}{c_p} \left(\frac{\partial u}{\partial y} \right)^2$$

Using the following transformations:

$$\eta = y \sqrt{\frac{a(n+1)}{2\upsilon}} x^{\frac{(n-1)}{2}}, \quad u = ax^n f'(\eta),$$

$$v = -\sqrt{\frac{a\upsilon(n+1)}{2}} x^{\frac{(n-1)}{2}} \left(f(\eta) + \frac{n-1}{n+1} \eta f'(\eta) \right) \tag{11}$$

$$G(\eta) = \frac{(T - T_\infty)}{(T_w - T_\infty)}, \quad H(\eta) = \frac{(C - C_\infty)}{(C_w - C_\infty)}$$

where ψ represent the stream function and is defined as:

$$u = \frac{\partial \psi}{\partial y} \quad and \quad v = -\frac{\partial \psi}{\partial x}$$

so that Eq.(1) is satisfied identically.

The governing equations (2), (10) and (4) are reduced by using equation (11) as follows:

$$f''' + ff'' - Nf'^2 - Mf' = 0 \quad (12)$$

$$\left(1 + \frac{4}{3}R\right)G'' + \Pr fG' + \Pr NbG'H'$$
$$+ \Pr NtG'^2 + \Pr Ecf''^2 = 0 \quad (13)$$

$$H'' + LefH' + \frac{Nt}{Nb}G'' = 0 \quad (14)$$

The transformed boundary conditions are:

$$f'(0) = 1 + Af''(0) + Bf'''(0),$$
$$f(0) = s, \ G(0) = 1 + EG'(0),$$
$$H(0) = 1 + DH'(0) \quad (15)$$
$$f'(\infty) = 0, \ G(\infty) = 0, \ H(\infty) = 0$$

where the prime denote differentiation with respect to η. The involved physical parameters are defined as follows:

$$N = \frac{2n}{n+1}, \ \Pr = \frac{\upsilon}{\alpha}, \ R = \frac{4\sigma^* T_\infty^3}{k^* \alpha (\rho C)_p},$$

$$Nb = \frac{\tau D_B (C_w - C_\infty)}{\upsilon}, \ Nt = \frac{\tau D_T (T_w - T_\infty)}{T_\infty \upsilon},$$

$$Ec = \frac{u_w^2}{C_p(T_w - T_\infty)} \quad M = \frac{2\sigma B_0^2}{a\rho_f (n+1)},$$

$$Le = \frac{\upsilon}{D_B}, \ s = \frac{-v_w}{x^{\frac{n-1}{2}}\sqrt{\frac{a\upsilon(n+1)}{2}}},$$

$$(16)$$

$$A = A'\sqrt{\frac{a(n+1)}{2}}x^{\frac{n-1}{2}} = \frac{2}{3}\left(\frac{3 - \alpha l^3}{\alpha} - \frac{3}{2}\frac{1-\alpha^2}{k_n}\right)\gamma\sqrt{\frac{a(n+1)}{2}}x^{\frac{n-1}{2}},$$

$$B = B'\frac{a(n+1)}{2}x^{n-1} = -\frac{1}{4}\left(l^4 + \frac{2}{k_n^2}(1-l^2)\right)\gamma^2\frac{a(n+1)}{2}x^{n-1},$$

$$E = k_1\sqrt{\frac{a(n+1)}{2}}x^{\frac{n-1}{2}}, \ D = k_2\sqrt{\frac{a(n+1)}{2}}x^{\frac{n-1}{2}}$$

Here N is the Power-law parameter, Pr is the Prandtl number, R is Thermal radiation, Nb is Brownian motion parameter, Nt is Thermophoresis parameter, Ec is Eckert number, M is Magnetic parameter, Le is Lewis number, s is mass transfer parameter, i.e., suction for $(v_w < 0)$, injection for $(v_w > 0)$, A is First order velocity slip parameter, B is second order velocity slip parameter, E is Thermal slip parameter, D is Concentration slip parameter.

Now equations (12) to (14) together with the boundary conditions (15) to have similarity solutions, the quantities A, B, E and D must be constant and not a function of 'x' as in equation (16). This condition can be realized if the mean free path of the nanoparticles γ is proportional to:

$$\gamma = cx^{\frac{-(n-1)}{2}}$$

We therefore assume:

$$\gamma = cx^{\frac{-(n-1)}{2}}, \ also \ assume \ thermal \ slip \ factor \ k_1 = e_1 x^{\frac{-(n-1)}{2}},$$
$$concentration \ slip \ factor \ k_2 = e_2 x^{\frac{-(n-1)}{2}} \quad (17)$$

C, k1, k2 are proportionality constants. With the introduction of (17) into equation (16) of velocity, thermal, concentration slip parameters, we have:

$$A = \frac{2}{3}\left(\frac{3 - \alpha l^3}{\alpha} - \frac{3}{2}\frac{1-l^2}{k_n}\right)\sqrt{\frac{a(n+1)}{2}}c > 0,$$

$$B = \frac{-1}{8}\left(l^4 + \frac{2}{k_n^2}(1-l^2)\right)a(n+1)c^2 < 0 \quad (18)$$

$$E = \sqrt{\frac{a(n+1)}{2}}e_1 > 0, \ D = \sqrt{\frac{a(n+1)}{2}}e_2 > 0$$

With A, B, E and D defined by equation (18), the solutions of equations (12) to (14) yield the similarity solutions. However, with A, B, E and D defined by relations (17), the solutions generated are the local similarity solutions. The quantities of practical interest, in the present study, are the local skin friction Cf$_x$, Nusselt number Nux and the Sherwood number Shx which are defined as:

$$C_f = \frac{\tau_w}{\rho u_w^2}, \ Nu_x = \frac{xq_w}{k(T_w - T_\infty)}, \ Sh_x = \frac{xq_m}{D_B(C_w - C_\infty)} \quad (19)$$

where τ_w is shear stress at wall, q_w is the heat flux and q_m is the mass flux at the surface which are given below:

$$\tau_w = \mu\left(\frac{\partial u}{\partial y}\right)_{y=0}, \ q_w = -\left(k + \frac{16\sigma^* T_\infty^3}{3k^*}\right)\left(\frac{\partial T}{\partial y}\right)_{y=0}, \ q_m = -D_B\left(\frac{\partial C}{\partial y}\right)_{y=0} \quad (20)$$

Substituting equation (10) into equations (19), (20), we obtain:

$$C_f \text{Re}^{\frac{1}{2}} = f''(0), \ Nu_x \text{Re}^{\frac{-1}{2}} = -\left(1 + \frac{4}{3}R\right)G'(0), \ Sh_x \text{Re}^{\frac{-1}{2}} = -H'(0) \quad (21)$$

$$where \ \text{Re} = \frac{a(n+1)}{2\upsilon}x^{n+1} \ Local \ \text{Reynods number}$$

3. Numerical Methods

The ordinary differential equations (12), (13), (14) with the boundary conditions of equation (15) are solved numerically by using of Keller-Box method, as revealed by [31], the following few steps are involved to achieve Numerical solutions:

- Reduce the above mentioned higher order ordinary differential equations into a system of first order ordinary differential equations;
- Write the finite differences for the first order equations;
- Linearize the algebraic equations by Newton's method, and write them in matrix–vector form; and
- Solve the linear system by the block tri-diagonal elimination technique.

- To get the accuracy of this method the appropriate initial guesses have been chosen. The following initial guesses are chosen:

$$f_0(\eta) = s + \frac{1}{1+A-B}\left(1-e^x\right), \quad G_0(\eta) = \left(\frac{1}{1+E}\right)e^{-x}, \quad H_0(\eta) = \left(\frac{1}{1+D}\right)e^{-x}$$

The choices of the above initial guesses depend on the convergence criteria and the transformed boundary conditions of equation (15). The step size 0.01 is used to obtain the numerical solution with four decimal place accuracy as the criterion of convergence.

4. Results and Discussion

The magneto hydrodynamics (MHD) boundary layer flow [32] and heat transfer [33] of a nanofluid with velocity second order slip, temperature jump, solutal boundary slip condition, suction and thermal radiation has been investigated numerically over a nonlinear stretching sheet with viscous dissipation. The numerical solutions are obtained for velocity, temperature and concentration profiles for different values of governing parameters. The obtained results are displayed through Figures 2 to 20 for velocity, temperature and concentration profiles, respectively. In the simulation the default values of the parameters are considered as M=1, Nb=Nt=0.5, Le=5, Pr=6.8, s=0.5, Ec=0.2, A=1, B=-1, E=1, D=1, R=0.1, N=1.5, unless otherwise specified.

5. Velocity Profiles

The velocity profile $f'(0)$ for different values of the magnetic field parameter M, mass suction parameter s, power-law parameter N and velocity first and second order slip parameter A, B are shown in Figures 2 to 6, respectively.

Figure 2 reveals the influences of magnetic field on the flow field. The presence of transverse magnetic field, the fluid induces Lorentz force, which opposes the flow. This resistive force tends to slow down the flow, which results in the decreasing of velocity field. As The values of magnetic parameter M increase, the retarding force increases and consequently the velocity decreases. The graph also reveals that the boundary layer thickness reduces as magnetic parameter M increases.
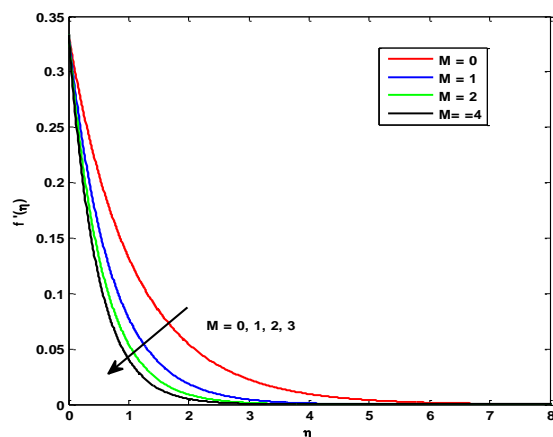

Figure 2. Velocity graph for different values of magnetic parameter M

The effect of suction/injection parameter 's' on the velocity profile for a nonlinear stretching surface is presented in Figure 3 in presence of surface slip. It is observed from the figure that velocity distribution across the boundary layer decreases with an increase in suction parameter s. Thus, the suction reduces the thickness of hydrodynamic boundary layer; the effect is reverse in the case of injection.
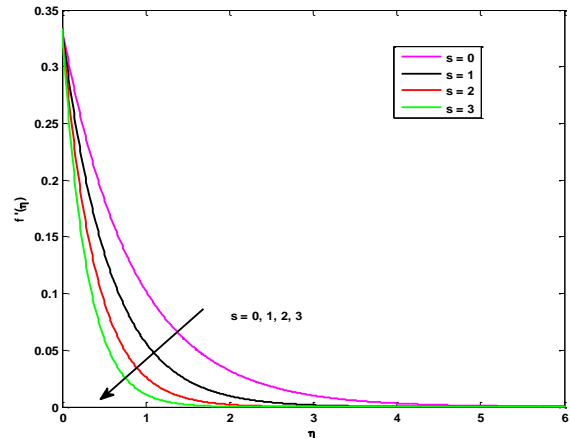

Figure 3. Velocity graph for different values of Suction parameter s.

On observing from Figure 4, as the power-law parameter increases, the velocity profile decreases. Figure 5 illustrates the variation of the dimensionless velocity component $f'(\eta)$ for various values of the first order slip parameter A. From the figure, it is clear that the velocity of the fluid near the boundary layer region decreases by increasing slip parameter. If the slip parameter increases, the slip at the surface wall is also increases. As a result it reaches to a smaller amount of diffusion due to the stretching surface into the fluid. In the case of no slip condition, the value of A approaches to zero so the velocity slip at the wall is equal to zero, i.e., $u_s = 0$, consequently the fluid velocity adjacent to the wall is equal to the velocity of the stretching surface u_w, then $f'(0) = 1$. Figure 6 shows that the dimensionless velocity component $f'(\eta)$ decreases with the decreasing values of second order velocity slip parameter B.
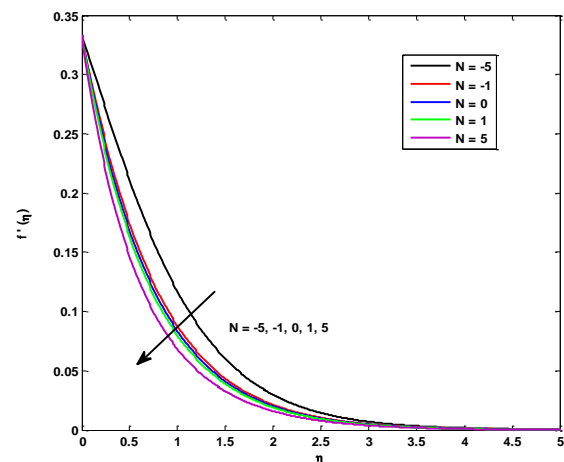

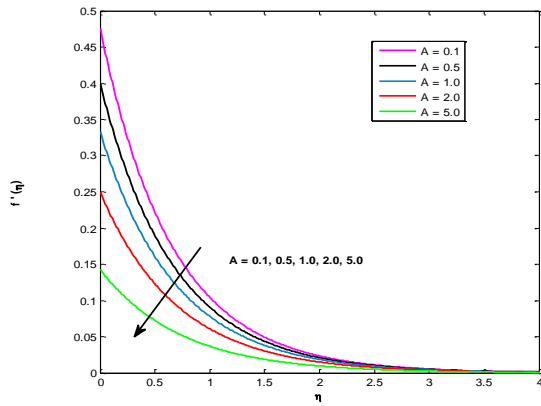**Figure 4.** Velocity graph for different values of Power-law parameter N

Figure 5. Velocity graph for different values of first order velocity slip parameter A
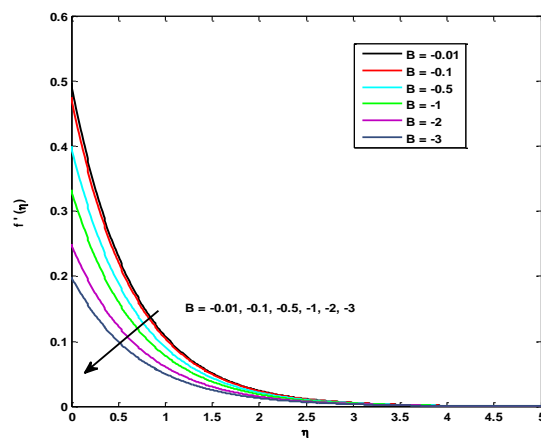

Figure 6. Velocity graph for different values of second order velocity slip parameter

6. Temperature Profiles

Figures 7 to 14 present the variation of temperature with respect to the governing parameters, viz. Prandtl number Pr, thermal slip parameter E, radiation parameter R, Eckert number Ec, suction parameter s, thermophoresis parameter Nt, Brownian motion parameter Nb and magnetic parameter M, respectively.

The effect of Prandtl number Pr on the heat transfer process is shown by the Figure 7. The Prandtl number is a material property, it varies from fluid to fluid. The Figure 7 reveals that as an increase in Prandtl number Pr, the temperature field decreases. An increase in the values of Pr reduces the thermal diffusivity, because Prandtl number is a dimensionless number which is defined as the ratio of momentum diffusivity to thermal diffusivity, that is $Pr = \upsilon/\alpha$. Increasing the values of Pr implies that momentum diffusivity is higher than thermal diffusivity. Therefore thermal boundary layer thickness is a decreasing function of Pr. In general the Prandtl number is used in heat transfer problems to reduce the relative thickening of the momentum and the thermal boundary layers.

The influence of thermal slip on the temperature profiles is shown in Figure 8 which describes that the fluid temperature decreases on increasing thermal slip parameter E in the boundary layer region and, as a consequence, thickness of the thermal boundary layer decreases.

Figure 9 demonstrates the variation of temperature with respect to radiation parameter *R*. When the Rosseland radiative absorptivity k^* decreases, the divergence of the radiative heat flux $\partial qr / \partial y$ increases, which leads to increases the rate of radiative heat transfer to the fluid at the surface, i.e., it provides more heat to the fluid which causes the fluid temperature to increase. Hence, the temperature profile as well as thermal boundary layer thickness increases as the value of thermal radiation increases.

Figure 10 illustrates the power of Eckert number Ec on temperature in the boundary layer. On observing the temperature graph, the wall temperature of the sheet increases as the values of Ec increase. As the irreversible process by means of which the work done by a fluid on adjacent layers due to the action of shear forces is transformed into heat influenced by viscous dissipation. It is also noticed that the reversal flow happened because of the temperature enhancement occurs as heat energy is stored in the fluid due to frictional heating. Also, due to the fact that, decrease of rate of heat transfer at the surface, the thermal boundary layer thickness increases, when the values of Ec increases.

In Figure 11 the influence of the suction/injection parameter 's' on the temperature profiles is depicted. It can, easily, be seen from the figure that the temperature distribution across the boundary layer decreases with increasing the values of s > 0 in the presence of thermal slip and hence the thickness of the thermal boundary layer decreases whereas opposite effect occurs for s < 0.

Figures 12 and 13 show the influence of the change of Brownian motion parameter Nb and thermophoresis parameter Nt on temperature profile. It is noticed that as thermophoesis parameter and Brownian motion parameter Increases the temperature increases in the boundary layer. As the thermophoretic effect increases, nanoparticles are migrated from the hot surface to cold ambient fluid, as a result the temperature will enhances in the boundary layer. This will help in the thickening of the thermal boundary layer. Figure 14 shows the influence of magnetic field parameter M on the thermal field. Transverse magnetic field has increased the thermal boundary layer thickness, so it causes the temperature increment in the boundary layer when it increases.
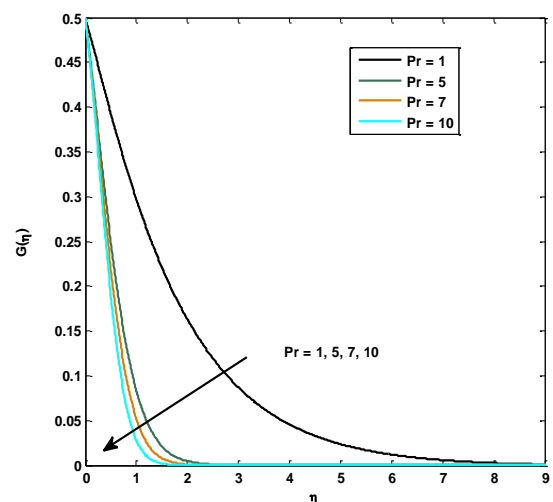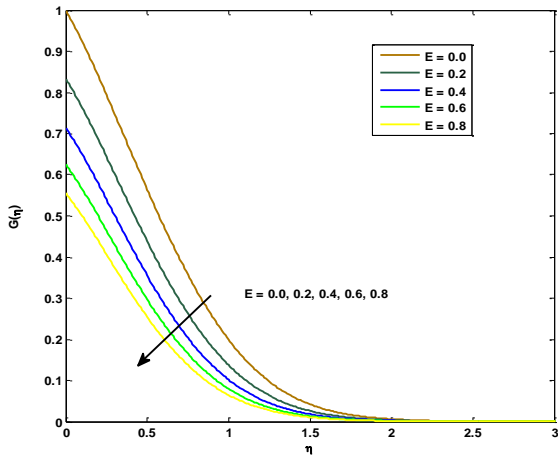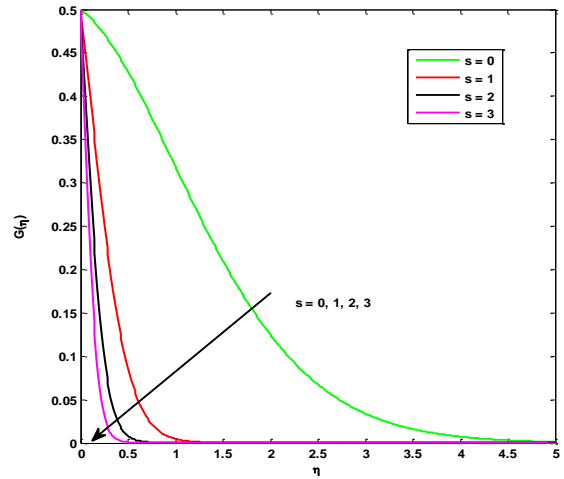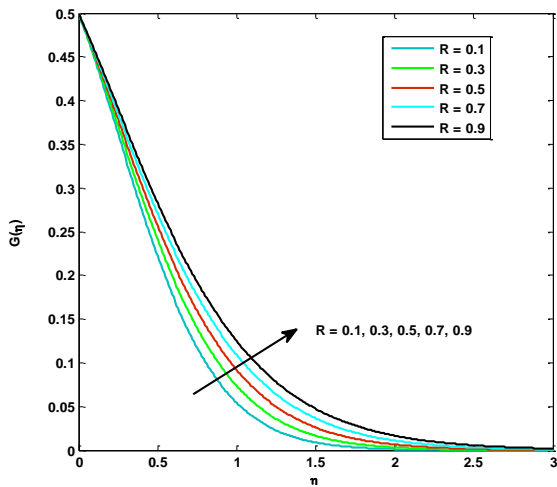

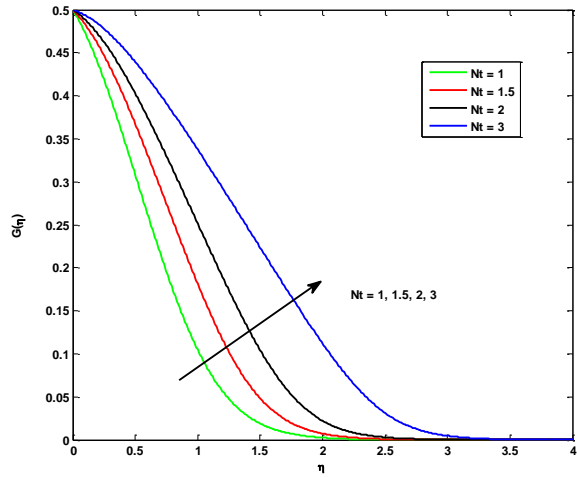**Figure 7.** Temperature graph for different values Prandtl number Pr

Figure 8. Temperature graph for different values Thermal slip parameter E

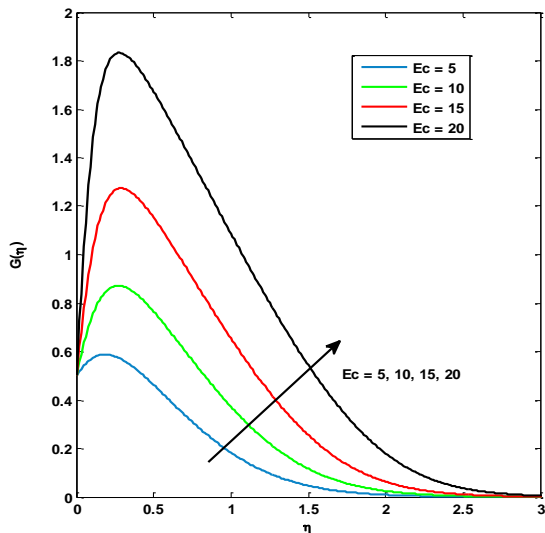

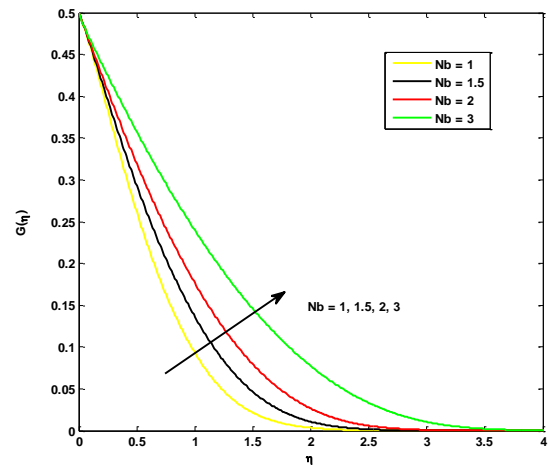**Figure 11.** Temperature graph for different values suction parameter s

Figure 9. Temperature graph for different values Thermal radiation R

Figure 12. Temperature graph for different values thermophoresis parameter Nt

Figure 10. Temperature graph for different values Eckert number Ec

Figure 13. Temperature graph for different values Brownian motion parameter Nb
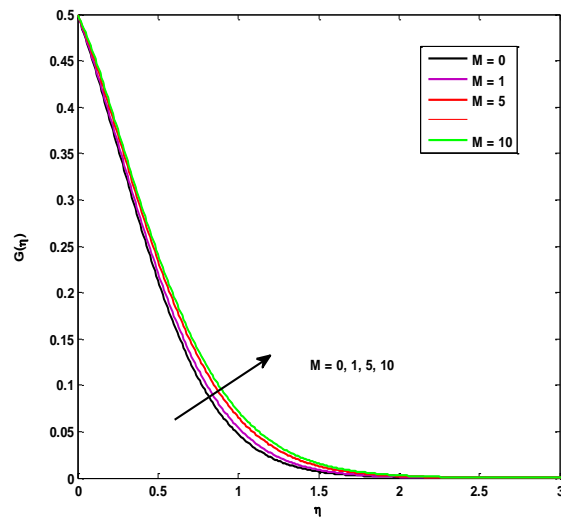
Figure 14. Temperature graph for different values magnetic parameter M

7. Nanoparticle Concentration Profiles

Figures 15 to 20 demonstrate the variation of nanoparticle concentration with respect to the change in governing parameters, viz. Lewis number Le, Brownian motion parameter Nb, thermophoresis parameter Nt, concentration slip parameter D, suction s and radiation parameter R.

Figure 15 shows the impact of Lewis number Le on concentration profile. Actually, a higher value of Lewis number Le $=\alpha/D_B$ represents a lower nanoparticle diffusivity (Brownian motion) and a higher thermal diffusivity. If Le > 1 the thermal diffusion rate exceeds the Brownian diffusion rate. Lower Brownian diffusion leads to less mass transfer rate, as a result, the nanoparticle volume fraction (concentration) graph and the concentration boundary layer thickness decreases. Figure16 reveals the variation of concentration profile. As the larger thermophoresis parameter Nt values gives the larger temperature gradient. The concentration field is motivated by the temperature gradient. As the temperature is an increasing function of Nt, an increase in Nt parameter increases the concentration and its boundary layer thickness. The nanoparticle concentration and concentration boundary layer thickness will increases as increase in Nt. We can see from the Figure 17 that the concentration profile is decreasing function of Nb. This may be due to the fact that as Brownian motion parameter decreases the mass transfer of a nanofluid.

From Figure 18 we can observe the variation of concentration with respect to solutal slip parameter D. As it can be seen from the graph, increasing in the concentration slip parameter D, the concentration profile is decreasing. The suction parameter 's' has a strong influence on the concentration profile as it is shown in Figure 19. As the values of suction parameter s increase, concentration graph decreases and the concentration boundary layer thickness decreases. Figure 20 reflects the variation of radiation on concentration graph. The influences of radiation parameter on concentration is not this much significant. As the values of radiation parameter

R increase, the concentration boundary layer thickness is not changing much, almost it is constant.

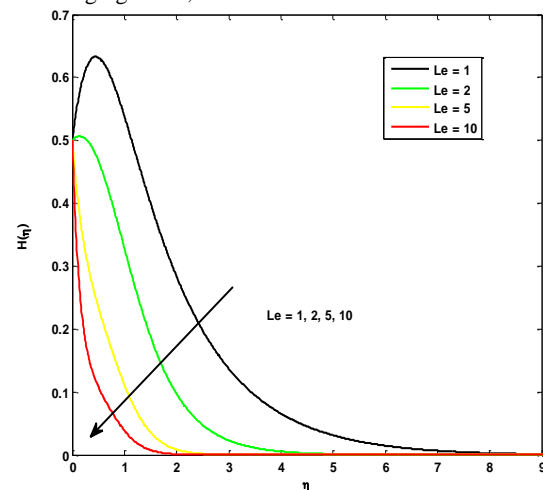

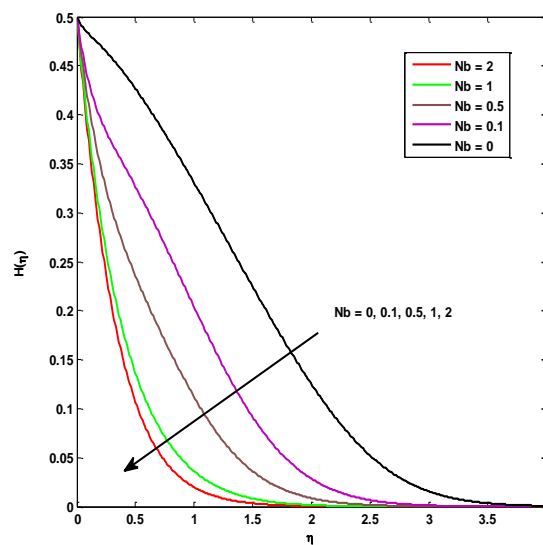**Figure 15.** Temperature graph for different values Lewis number Le

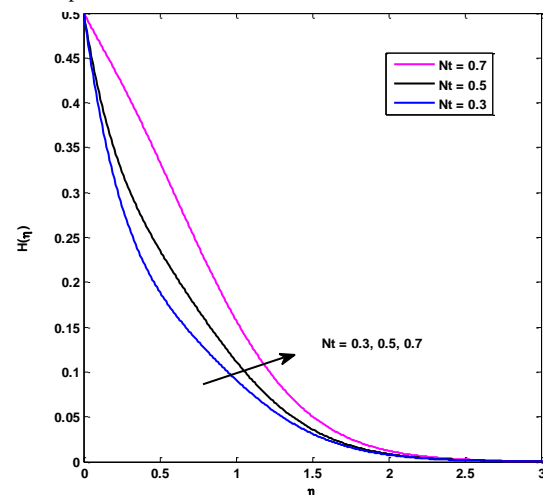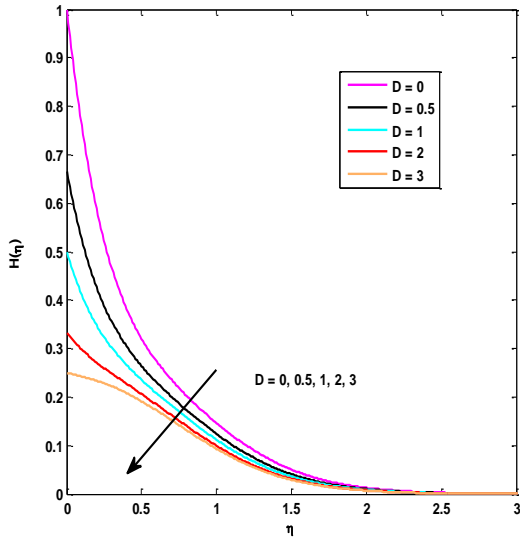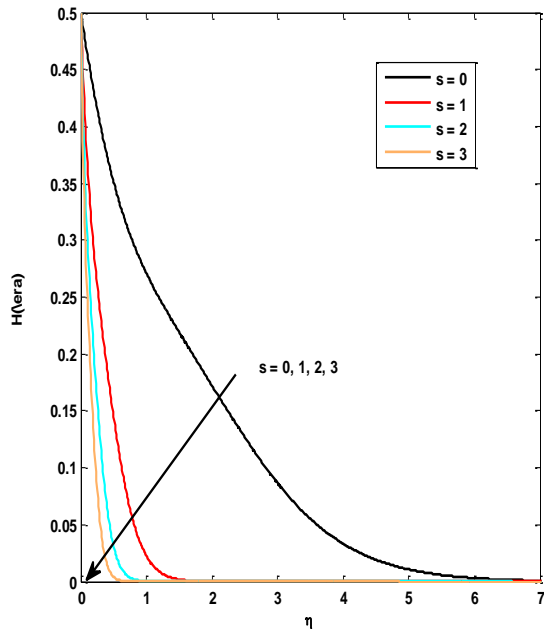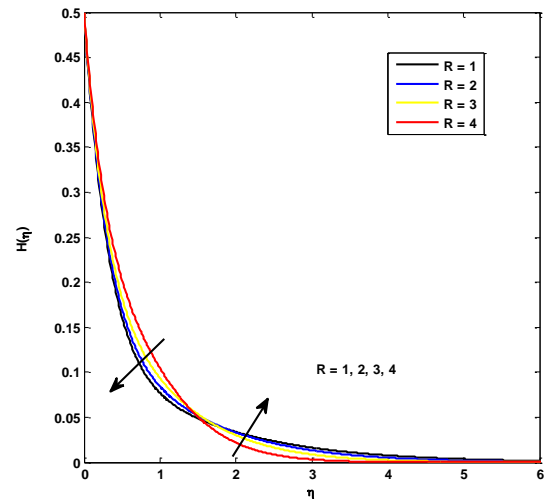**Figure 16.** Temperature graph for different values Brownian motion parameter Nb

Figure 17. Temperature graph for different values thermophoresis parameter Nt

Figure 18. Temperature graph for different values concentration slip parameter D

Figure 19. Temperature graph for different values suction parameter s

Figure 20. Temperature graph for different values thermal radiation R

Finally, a comparison is done with previous results as it is shown in Table 1, for the numerical values of the skin friction coefficient $-f''(0)$, local Nusselt number $-G'(0)$ and Sherwood number $-H'(0)$ when slip parameters A, B, E, D radiation parameter R and suction parameter s are absent. And it is in excellent agreement with the result published in F. Mabood *et al.* 2015. Table 2 presents the variation of the skin friction coefficient in relation to magnetic field M, suction s, power-law parameter N and velocity first and second order slip parameters A, B. On observing this table, as the values of magnetic field, suction and power-law parameters increase, the values of skin friction coefficient increase. However, the skin friction coefficient decreases as both the values of velocity slip parameters A and B increase. Table 3 shows the local Nusselt number $-G'(0)$ and Sherwood number $-H'(0)$ for different values of Prandtl number Pr, thermal radiation R, Eckert number Ec, thermal slip parameter E and concentration parameter D. It is possible to see that as the values of Prandtl number increase, the heat transfer rate (local Nusselt number) is increased, but when other values as indicated in Table 3 increases, the local Nusselt number decreases. Also we can observe the variation of the mass transfer rate i.e., Sherwood number from this Table. Table 4 represents the variation of both the heat transfer rate $-G'(0)$ and mass transfer rate $-H'(0)$ for different values of the parameters M, s, Nt, Nb and Le when other parameters are fixed.

Table 1. Comparison of Skin friction coefficient, Nusselt and Sherwood numbers when A = B = E = D = R = s = 0

Ec	M	$-f''(0)$ (F.Mabood et al, 2015)	$-f''(0)$ (Present)	$-G'(0)$ (F.Mabood et al, 2015)	$-G'(0)$ (Present)	$-H'(0)$ (F.Mabood et al, 2015)	$-H'(0)$ (Present)
0	0	1.10102	1.1010	1.06719	1.0672	1.07719	1.0772
0.1				0.88199	0.8892	1.22345	1.2234
0.2				0.70998	0.7100	1.37078	1.3708
0.3				0.52953	0.5295	1.51919	1.5192
0.5				0.16484	0.1648	1.81933	1.8194
0	0.5	1.3098	1.3099	1.04365	1.0473	1.01090	1.0109
0.1				0.81055	0.8106	1.20605	1.2060
0.2				0.57564	0.5757	1.40279	1.4028
0.3				0.33889	0.3389	1.60115	1.6012
0.5				0.14022	0.1402	2.00282	2.0028
0	1	1.48912	1.4891	1.02337	1.0234	0.95495	0.9549
0.1				0.74058	0.7406	1.19496	1.1950
0.2				0.45543	0.4554	1.43706	1.4371
0.3				0.16789	0.1679	1.68128	1.6813
0.5				0.41451	0.4145	2.17623	2.1763

Table 2. Calculation of skin friction coefficient for various values of M, s, A, B, N.

M	S	A	B	N	$-f''(0)$
0	0.5	1	-1	1,5	0.3170
0.5					0.4161
1.0					0.4914
1.5					0.5547
2.0					0.6105
1.0	0				0.4005
	0.2				0.4348
	0.7				0.5325
	1.0				0.5988
	0.5	1			0.4914
		1.2			0.4572
		1.3			0.4418
		1	-1		0.4914
			-2		0.3572
			-3		0.2801
			-1	-0.5	0.4314
				0.5	0.4624
				1.5	0.4914

Table 3. Calculation of Nussult and Sherwood numbers for various values of Pr, R, Ec, E, D.

Pr	R	Ec	E	D	- G ′(0)	- H ′(0)
1	0.1	0.2	1	1	0.2086	1.2676
5					0.4451	1.0703
7					0.4712	1.0505
10					0.4764	1.0508
6.8	0.5				0.4367	1.0771
	0.7				0.4188	1.0918
	1.0				0.3931	1.1131
	0.1	1			0.2470	1.2656
		2			0.0424	1.5440
		3			0.3457	1.8356
		0.2	0		0.6850	0.8984
			1		0.4677	1.0515
			2		0.3411	1.1538
			3		0.2610	1.2195
			1	0	0.1623	-2.7794
				1	0.4697	-1.0515
				2	0.6383	-0.4101
				3	0.7382	0.0740

Table 4. Calculation of Nussult and Sherwood numbers for various values of M, s, Le, Nb, Nt.

M	S	Le	Nb	Nt	-G ′ (0)	-H ′ (0)
0.1	0.5	5	0.5	0.5	0.4927	1.0677
0.2					0.4897	1.0648
0.3					0.4869	1.0623
0.4					0.4842	1.0601
1.0	-0.3				0.0378	0.0639
	-0.2				0.0180	0.1433
	-0.1				-0.0238	0.2541
	0.1				-0.1461	0.5105
	0.2				-0.2205	0.6428
	0.3				-0.3002	0.7771
	0.5	5			0.4697	1.0515
		10			0.3349	2.4995
		15			0.2861	3.8315
		20			0.2610	5.1277
		5	0.1		0.7194	1.3103
			0.2		0.6351	1.2183
			0.3		0.5676	1.1489
			0.4		0.5133	1.0951
			0.5	0.1	2.7662	11.8889
				0.2	1.1371	1.1609
				0.3	0.7582	-0.3290
				0.4	0.5792	-0.8239

8. Conclusions

A numerical study was investigated for the radiative boundary layer flow and heat transfer of nanofluids over a nonlinear stretching sheet with slip conditions, suction with the help of an implicit finite difference method known as Keller-Box method. A parametric study is performed to explore the effects of various governing parameters on the fluid flow and heat transfer characteristic.

The following conclusions give a brief account of the results of the present study:

1. Both first and second order velocity slip parameter A and B reduces the thickness of momentum boundary layer and hence decrease the velocity. N decreases the velocity profile.
2. Velocity profile decrease with increase in suction parameter s, magnetic parameter M.
3. Prandtl number Pr, thermal slip parameter E, suction parameter s reduces the temperature profile.
4. The temperature increases with an increase in radiation parameter R, magnetic parameter M, thermophorosis parameter Nt, Brownian motion parameter Nb, Eckert number Ec.
5. Concentration profile decreases with an increase in Lewis number Le, Brownian motion parameter Nb, concentration slip parameter D, suction s and radiation R but increases with an increase in thermophorosis parameter Nt.

Acknowledgements

References

[1] T. Fang, S. Yao, J. Zhang, A. Aziz, "Viscous flow over a shrinking sheet with a second order slip flow model". Comm. Nonlinear Sci. Num. Simul, Vol. 15 (2010), 1831–1842.

[2] T. Fang, A. Aziz, "Viscous flow with second-order slip velocity over a stretching sheet". Natur forsch. A – Phys. Sci. Vol. 65a (2010), 1087–1092.

[3] Mahantesh, M. Nandeppanavar, K. Vajravelu, M. Subhas Abel, M.N. Siddalingappa, "Second order slip flow and heat transfer over a stretching sheet with non-linear Navier boundary condition". Int. J. of Ther. Sci., Vol. 58 (2012), 143-150.

[4] Rosca, C. Natalia, Ioan Pop, "Mixed convection stagnation point flow past a vertical flat plate with a second order slip: Heat flux case". Int. J. of Heat and Mass Transfer, Vol. 65 (2013), 102–109.

[5] Rosca, V. Alin, Ioan Pop, "Flow and heat transfer over a vertical permeable stretching/shrinking sheet with a second order slip". Int. J. of Heat and Mass Transfer, Vol. 60 (2013), 355–364.

[6] M. M. Khader, "Laguerre collocation method for the flow and heat transfer due to a permeable stretching surface embedded in a porous medium with a second order slip and

[7] A. K. Abdul Hakeem, N. Vishnu Ganesh, B. Ganga, "Magnetic field effects on second order slip flow of nanofluid over a stretching/shrinking sheet with thermal radiation effect". J. Mag. and Mag. Mat., Vol. 381 (2015), 243–257.

[8] F. Mabood, A. berardino, "Melting heat transfer on MHD convective flow of a nanofluid over a stretching sheet with viscous dissipation and second order slip". J. Taiwan Inst. Chem. Eng. Vol. 374 (2015), 1–7.

[9] T. Hayat, T. Muhammad, A. Alsaedi, M.S. Alhuthali, "Magnetohydrodynamic three-dimensional flow of viscoelastic nanofluid in the presence of nonlinear thermal radiation". J. Mag. and Mag. Mat.,Vol. 385 (2015), 222–229.

[10] J. Zhu, L. Zheng, L. Zheng and X. Zhang, "Second-order slip MHD flow and heat transfer of nanofluids with thermal radiation and chemical reaction". Appl. Math. and Mech., Vol. 36 (2015) No. 9, 1131-1146.

[11] A. M. Megahed, "MHD viscous Casson fluid flow and heat transfer with second-order slip velocity and thermal slip over a permeable stretching sheet in the presence of internal heat generation/absorption and thermal radiation". The Eur.Phy. J. Plus, Vol. 130 (2015), 81.

[12] S. U. S. Choi, "Enhancing thermal conductivity of fluids with nanoparticles". Dev. Appl Non-Newton Flows, Vol. 66 (1995), 99–105.

[13] J. Buongiorno, L. W. Hu, "Nanofluid coolants for advanced nuclear power plants". Proceedings of ICAPP 2005, Seoul, Paper no. 5705 (2005), 15–19.

[14] K. N. Shukla, A, B. Solomon, B.C. Pillai, "Thermal performance of cylindrical heat pipe using nanofluids" J. Ther. Heat Transfer, Vol. 24 (2010), 796–802.

[15] W. A. Khan, I. Pop, "Boundary layer flow of a nanofluid past a stretching sheet". Int. J. Heat Mass Trans, Vol. 53 (2010), 2477–2483.

[16] S. Nadeem, C. Lee, "Boundary layer flow of a nanofluid over an exponentially stretching surface". Nanoscale Res Lett., Vol. 7 (2012), 94.

[17] P. Rana, R. Bhargava, "Flow and heat transfer of a nanofluid over a nonlinear stretching sheet: A numerical study". Commun Nonlin Sci Numer Simul, Vol. 17 (2012), 212–226.

[18] M. M. Rahmann, I.A. Eltayeb, "Radiative heat transfer in a hydromagnetic nanofluid past a nonlinear stretching surface with convective boundary condition". Meccanica, Vol. 48 (2013), 601–615.

[19] R. Cortell, "Effect of viscous dissipation and radiation on the thermal boundary layer over a non-linearly stretching sheet". Phys Lett A, Vol. 372 (2008), 631–636.

[20] T. G. Motsumi, O.D. Makinde, "Effects of thermal radiation and viscous dissipation on boundary layer flow of nanofluids over a permeable moving flat plate". Phys Script, Vol. 86 (2012), 045003.

[21] [21] D. Pal, G. Mandal, K. Vajravelu, "MHD convection–dissipation heat transfer over a non-linear stretching and shrinking sheets in nanofluids with thermal radiation". Int. J. Heat Mass Trans., Vol. 65 (2013), 481–90.

[22] S. K. Nandy, I. Pop, "Effects of magnetic field and thermal radiation on stagnation flow and heat transfer of nanofluid over a shrinking surface". Int. Comm. Heat Mass Trans., Vol. 53 (2014), 50–55.

[23] M. M. Rashidi, N. V. Ganesh, A.K.A. Hakeem, B. Ganga, "Buoyancy effect on MHD flow of nanofluid over a stretching sheet in the presence of thermal radiation". J Mol. Liq., Vol. 198 (2014), 234–238.

[24] M. Mustafa, T. Hayat, S. Obaidat, "Boundary layer flow of a nanofluid over an exponentially stretching sheet with convective boundary conditions". Int. J. Num. Met. Heat Fluid Flow, Vol. 23 (2013), 945–959.

[25] S. Nadeem, T. Hayat, M.Y. Malik, S.A. Rajput, "Thermal radiations effects on the flow by an exponentially stretching surface: a series solution", Natur forsch. Vol. 65A (2010), 1–9.

[26] S. Nadeem, C. Lee, "Boundary layer flow of nanofluid over an exponentially stretching surface". Nanoscale Res. Lett. Vol. 7 (2012), 94-100.

[27] K. Bhattacharyya, "Boundary layer flow and heat transfer over an exponentially shrinking sheet". Chin. Phys. Lett. Vol. 28 (2011), 074701.

[28] K. Bhattacharyya, K. Vajravelu, "Stagnation-point flow and heat transfer over an exponentially shrinking sheet", Comm. Nonlinear Sci. Numer. Simul., Vol. 17 (2012), 2728–2734.

[29] L. Wu, "A slip model for rarefied gas flows at arbitrary Knudsen number". Appl. Phys. Lett., Vol. 93 (2008), 253-103.

[30] Rosseland S, Astrophysik und atom-theoretische Grundlagen, Berlin: Springer; 1931.

[31] Cebeci T, Bradshaw P., Physical and Computational Aspects of Convective Heat Transfer, Berlin: Springer; 1988.

[32] Z. Uddin, M. Kumar, "MHD Heat and Mass Transfer Free Convection Flow near The Lower Stagnation Point of an Isothermal Cylinder Imbedded in Porous Domain with the Presence of Radiation". Jordan Journal of Mechanical and Industrial Engineering, Vol. 5 (2011) No. 2, 133-138.

[33] I. Zahmatkesh, "Heatline Visualization of Buoyancy-Driven Flow inside a Nanofluid-Saturated Porous Enclosure". Jordan Journal of Mechanical and Industrial Engineering, Vol. 9 (2015) No.2, 149-157.